

Accepted Manuscript

Synthesis, molecular modeling studies and evaluation of antifungal activity of a novel series of thiazole derivatives

Cleudiomar Inácio Lino, Igor Gonçalves de Souza, Beatriz Martins Borelli, Thelma Tirone Silvério Matos, Iasmin Natália Santos Teixeira, Jonas Pereira Ramos, Elaine Maria de Souza Fagundes, Philippe de Oliveira Fernandes, Vinícius Gonçalves Maltarollo, Susana Johann, Renata Barbosa de Oliveira



PII: S0223-5234(18)30326-X

DOI: [10.1016/j.ejmech.2018.03.083](https://doi.org/10.1016/j.ejmech.2018.03.083)

Reference: EJMECH 10348

To appear in: *European Journal of Medicinal Chemistry*

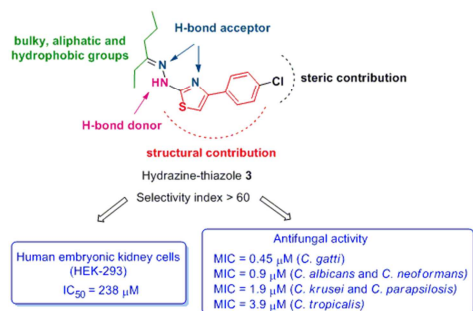
Received Date: 12 October 2017

Revised Date: 2 March 2018

Accepted Date: 30 March 2018

Please cite this article as: Cleudiomar.Iná. Lino, I. Gonçalves de Souza, B.M. Borelli, T.T. Silvério Matos, Iasmin.Natá. Santos Teixeira, J.P. Ramos, E. Maria de Souza Fagundes, P. de Oliveira Fernandes, Viní.Gonç. Maltarollo, S. Johann, R.B. de Oliveira, Synthesis, molecular modeling studies and evaluation of antifungal activity of a novel series of thiazole derivatives, *European Journal of Medicinal Chemistry* (2018), doi: 10.1016/j.ejmech.2018.03.083.

This is a PDF file of an unedited manuscript that has been accepted for publication. As a service to our customers we are providing this early version of the manuscript. The manuscript will undergo copyediting, typesetting, and review of the resulting proof before it is published in its final form. Please note that during the production process errors may be discovered which could affect the content, and all legal disclaimers that apply to the journal pertain.



ACCEPTED MANUSCRIPT

Synthesis, Molecular Modeling Studies and Evaluation of Antifungal Activity of a Novel Series of Thiazole Derivatives

Cleudiomar Inácio Lino^a, Igor Gonçalves de Souza^a, Beatriz Martins Borelli^b, Thelma Tirone Silvério Matos^b, Iasmin Natália Santos Teixeira^a, Jonas Pereira Ramos^c, Elaine Maria de Souza Fagundes^c, Philipe de Oliveira Fernandes^d, Vinícius Gonçalves Maltarollo^a, Susana Johann^b, Renata Barbosa de Oliveira^{a*}.

^aDepartamento de Produtos Farmacêuticos, Faculdade de Farmácia, Universidade Federal de Minas Gerais, Belo Horizonte, MG, Brazil.

^bDepartamento de Microbiologia, Instituto de Ciências Biológicas, Universidade Federal de Minas Gerais, Belo Horizonte, MG, Brazil.

^cDepartamento de Fisiologia e Biofísica, Instituto de Ciências Biológicas, Universidade Federal de Minas Gerais, Belo Horizonte, MG, Brazil.

^dDepartamento de Química, Instituto de Ciências Exatas, Universidade Federal de Minas Gerais, Belo Horizonte, MG, Brazil.

*Corresponding author: Tel.: +55-31-34096395; fax: +55-31-34096935. E-mail address: renatabo@farmacia.ufmg.br

Abstract

In the search for new antifungal agents, a novel series of fifteen hydrazine-thiazole derivatives was synthesized and assayed *in vitro* against six clinically important *Candida* and *Cryptococcus* species and *Paracoccidioides brasiliensis*. Eight compounds showed promising antifungal activity with minimum inhibitory concentration (MIC) values ranging from 0.45 to 31.2 μM , some of them being equally or more active than the drug fluconazole and amphotericin B. Active compounds were additionally tested for toxicity against human embryonic kidney (HEK-293) cells and none of them exhibited significant cytotoxicity, indicating high selectivity. Molecular modeling studies results corroborated experimental SAR results, suggesting their use in the design of new antifungal agents.

Keywords: antifungal agents; hydrazine-thiazoles; QSAR

1. Introduction

Over the last decades, there has been a significant increase in the incidence of fungal infections in humans, mainly affecting immunocompromised patients [1,2]. Among the fungi of clinical importance, pathogenic yeasts of the genus *Candida* and *Cryptococcus* are the most relevant [3], since candidemia is the third or fourth most common cause of healthcare-associated bloodstream infections in US hospitals [4]. Also in Brazil, mortality rates of candidemia can exceed more than half of the clinical cases [5,6]. The main pathogenic species of the genus *Candida* are *C. albicans*, *C. parapsilosis*, *C. tropicalis*, *C. glabrata*, *C. krusei*, *C. guilliermondii* and *C. lusitaniae*. Among those, *C. albicans* is the most frequently isolated agent of candidiasis, but non-*albicans* species of *Candida* have also increased their prevalence and gained clinical significance worldwide in the last years [7,8].

Cryptococcosis is an infectious disease with worldwide distribution and a wide array of clinical presentations caused by pathogenic encapsulated yeasts in the genus *Cryptococcus*, mainly *C. neoformans* and *C. gattii* [9]. Cryptococcal meningitis is one of the most important HIV related opportunistic infections and it is associated with significant mortality, approximately 181,100 deaths per year [10].

Paracoccidioidomycosis (PCM) is a disease mostly limited to Latin America and is caused by one of the two known species of the genus *Paracoccidioides*, *P. brasiliensis* and *P. lutzii*. PCM is the highest cause of mortality among systemic mycoses in Brazil, causing 1.65 deaths per 10⁶ inhabitants [11-13].

The treatment of fungal infections is very limited, when compared to bacterial infections, with only a limited number of available drugs. This is attributable to the nature of the fungal's cell that, as eukaryotic organisms, contain few drug targets not shared with human hosts [14]. Although much progress has been achieved in the development of therapeutic alternatives for treatment of these infections, the search for new antifungal compounds is still mandatory because of the serious side effects of available drugs and emergence of resistance [15].

Thiazole heterocycles constitute an interesting class of molecules, which exhibit a broad spectrum of biological activity, including antifungal properties [16-19]. Encouraged by our previous study that describes the activity of hydrazine-thiazole derivatives against *C. gattii* and *C. neoformans* [20], we decided to synthesize novel compounds of this class in order to investigate their activity against different species of fungi.

Additionally, 2D- and 3D-QSAR studies, as well as 3D similarity models, were constructed for prediction of biological activities and provide a basis for the design of novel compounds having improved potency.

2. Materials and Methods

2.1 Chemistry - All melting points were determined on a Microquímica MQAPF 301 apparatus. The IR spectra were recorded using a PerkinElmer Spectrum One infrared spectrometer and absorptions are herein reported as wave numbers (cm^{-1}). The NMR spectra were recorded on a Bruker AVANCE DRX200 instrument, using tetramethylsilane (TMS) as the internal standard. All reagents of analytical grade were obtained from commercial suppliers and used without further purification. The synthesis and the characterization of the ketones **16a** [21] and **17a** [22] and thiosemicarbazones **16b-22b** were previously reported in the literature [23-29], as well as the synthesis of the hydrazine-thiazoles **10** [26] and **11** [30].

2.1.1 General procedure for synthesis of hydrazine-thiazoles 1-15 [31]

To a solution of 1 equivalent of thiosemicarbazones **16b-22b** in isopropyl alcohol was added 1 equivalent of non-substituted or *para*-substituted 2-bromoacetophenone. The reaction mixture was kept under reflux and magnetic stirring for approximately 90 minutes. After the completion of the reaction (monitored by TLC), the mixture was then cooled to room temperature for precipitation. The precipitate was filtered and washed with saturated solution of NaHCO_3 followed by cold distilled water.

2.1.1.1 Synthesis of 2-[(2-(hexan-3-ylidene)hydrazo)-4-phenylthiazole (1)

Using the general procedure described above (section 2.1.1), **1** was obtained as a yellow solid in 94 % yield. Mp: 105.1-106.5 °C; IR (cm^{-1}): 2960, 2933, 2869, 1616, 1493, 1450; ^1H NMR (200 MHz, CDCl_3), δ/ppm : 13.8 (1H, s), 12.8 (1H, s), 7.7 (2H, m), 7.5 (3H, m), 6.7 (1H, s), 2.6-2.3 (4H, m), 1.8-1.6 (2H, m), 1.3-1.0 (6H, m); ^{13}C NMR (50 MHz, CDCl_3), δ/ppm : 170.1, 162.3, 145.0, 130.7, 129.2, 125.8, 102.0, 32.8, 30.0, 19.2, 14.3, 10.5; HRMS (m/z) 374.1372 $[\text{M}+\text{H}]^+$, calcd274.1378 $\text{C}_{15}\text{H}_{20}\text{N}_3\text{S}^+$.

2.1.1.2 Synthesis of 2-[(2-(hexan-3-ylidene)hydrazo)-4-(4-methoxyphenyl)-thiazole (2)

Using the general procedure described above (section 2.1.1), **2** was obtained as a pale solid in 97% yield. Mp: 106.8-107.4 °C; IR (cm^{-1}): 3504, 2960, 2934, 1607, 1590, 1508, 1455, 1256, 1188; ^1H NMR (200 MHz, CDCl_3), δ/ppm : 13.7 (1H, s), 12.4(1H, s), 7.6(2H, d), 6.9(2H, d), 6.5(1H, s), 3.8(3H, s), 2.6-2.3 (4H, m), 1.7-1.6(2H, m), 1.3-1.1(6H, m); ^{13}C NMR(50 MHz, CDCl_3), δ/ppm : 170.0, 165.2, 161.0, 141.8, 127.3, 121.3, 114.9, 99.3, 55.5, 38.0, 30.0, 33.3, 24.6, 19.4, 14.2, 13.7, 10.4, 10.1; HRMS (m/z) 304.1485 $[\text{M}+\text{H}]^+$, calcd304.1487 $\text{C}_{16}\text{H}_{22}\text{N}_3\text{OS}^+$.

2.1.1.3 Synthesis of 2-[(2-(hexan-3-ylidene)hydrazo]-4-(4-chlorophenyl)-thiazole (3)

Using the general procedure described above (section 2.1.1), **3** was obtained as a pale solid in 99 % yield. Mp: 148.2-149.1 °C; IR (cm⁻¹): 3156, 3108, 2961, 2931, 2871, 1558, 1477, 1457, 731; ¹H NMR (200 MHz, DMSO-d₆), δ/ppm: 13.8 (1H, s), 12.4 (1H, s), 7.7 (2H, d), 7.4 (2H, d), 6.8(1H, s), 2.6-2.3(4H, m), 1.7-1.6 (2H, m), 1.3-1.0 (6H, m); ¹³C NMR (50 MHz, DMSO-d₆), δ/ppm: 170.1, 167.3, 139.3, 136.5, 129.9, 127.0, 125.9, 101.8, 38.1, 30.1, 33.6, 25.0, 19.5, 19.4, 14.3, 13.8, 10.3; HRMS (m/z) 308.0983 [M+H]⁺, calcd 308.0988 C₁₅H₁₈ClN₃S⁺.

2.1.1.4 Synthesis of (E)-2-[2-(2,2-dimethylpropylidene)hydrazo]-4-phenylthiazole (4)

Using the general procedure described above (section 2.1.1), **4** was obtained as a violet solid in 90% yield. Mp: 101.2-102.1 °C; IR (cm⁻¹): 3062, 2959, 2901, 2865, 1626, 1603, 1584, 1576, 1483, 1443; ¹H NMR (200 MHz, DMSO-d₆), δ/ppm: 7.8-7.7 (3H, m), 7.4-7.3 (4H, m), 7.2 (1H, s), 1.1 (9H, s); ¹³C NMR (50 MHz, DMSO-d₆), δ/ppm: 169.1, 154.9, 148.1, 133.5, 128.7, 127.9, 125.7, 103.5, 34.6, 27.3; HRMS (m/z) 260.1216 [M+H]⁺, calcd 260.1221 C₁₄H₁₈N₃S⁺.

2.1.1.5 Synthesis of (E)-2-[2-(2,2-dimethylpropylidene)hydrazo]-4-(4-methoxyphenyl)-thiazole (5)

Using the general procedure described above (section 2.1.1), **5** was obtained as a pale solid in 94% yield. Mp: 104.5-105.8 °C; IR (cm⁻¹): 3061, 2960, 2836, 1624, 1574, 1510, 1493, 1462, 1248; ¹H NMR (200 MHz, DMSO-d₆), δ/ppm: 7.7 (2H, d); 7.5 (1H, s); 7.1 (1H, s); 6.9 (2H, d); 3.8 (3H, s); 1.1 (9H, s); ¹³C NMR (50 MHz, DMSO-d₆), δ/ppm: 169.1, 159.3, 155.9, 146.7, 127.2, 125.5, 114.1, 101.6, 55.2, 34.7, 27.2; HRMS (m/z) 290.1322 [M+H]⁺, calcd 290.1327 C₁₅H₂₀N₃OS⁺.

2.1.1.6 Synthesis of (E)-2-[2-(2,2-dimethylpropylidene)hydrazo]-4-(4-chlorophenyl)-thiazole (6)

Using the general procedure described above (section 2.1.1), **6** was obtained as a pale solid in 87 % yield. Mp: 148.5-149.6 °C; IR (cm⁻¹): 3162, 3116, 3078, 2963, 2863, 1568, 1479, 727; ¹H NMR (200 MHz, DMSO-d₆), δ/ppm: 11.6 (1H, s), 7.8 (2H, d), 7.4 (2H, d), 7.3(1H, s), 7.2 (1H, s), 1.1 (9H, s); ¹³C NMR (50 MHz, DMSO-d₆), δ/ppm: 169.0, 152.9, 149.0, 133.6, 131.8, 128.5, 127.2, 103.8, 34.4, 27.3; HRMS (m/z) 294.0826 [M+H]⁺, calcd 294.0832 C₁₄H₁₇ClN₃S⁺.

2.1.1.7 Synthesis of (E)-3-buten-2-one-4-(4-hydroxy-3-methoxyphenyl)-2-(4-phenyl-2-thiazolyl)hydrazone (7)

Using the general procedure described above (section 2.1.1), **7** was obtained as an orange solid in 76 % yield. Mp: 155.5-156.5 °C; IR (cm⁻¹): 3485, 3069, 2965, 1615, 1574, 1516, 1489, 1282, 1266; ¹H NMR (200 MHz, DMSO-d₆), δ/ppm: 11.1 (1H, s), 9.2 (1H, s), 7.8 (2H, d), 7.4-7.1 (5H, m), 7.0-6.8 (3H, m), 3.8 (3H, s), 2.1 (3H, s); ¹³C NRM (50 MHz, DMSO-d₆), δ/ppm: 169.2, 150.4, 148.7, 147.9, 147.2, 134.8, 132.3, 128.6, 128.0, 127.4, 125.5, 120.7, 115.6, 110.0, 103.8, 55.6, 12.3; HRMS (m/z) 366.1269 [M+H]⁺, calcd 366.1271 C₂₀H₂₀N₃O₂S⁺.

2.1.1.8 Synthesis of (*E*)-3-buten-2-one-4-(4-hydroxy-3-methoxyphenyl)-2-(4-(4-methoxyphenyl)-2-thiazolyl)hydrazone (**8**)

Using the general procedure described above (section 2.1.1), **8** was obtained as an orange solid in 82 % yield. Mp: 188-189.6 °C; IR (cm⁻¹): 3202, 3113, 2927, 2837, 1609, 1510, 1457, 1256; ¹H NMR (200 MHz, DMSO-d₆), δ/ppm: 11.1 (1H, s), 9.2 (1H, s), 7.8 (2H, d), 7.4-7.3 (2H, m), 7.2-6.9 (3H, m), 6.8-6.6 (3H, m), 3.8 (3H, s), 3.7 (3H, s), 2.1 (3H, s); ¹³C NRM (50 MHz, DMSO-d₆), δ/ppm: 169.0, 158.7, 150.2, 148.6, 147.8, 147.1, 132.2, 128.0, 127.6, 126.8, 125.7, 120.6, 115.6, 113.9, 110.0, 101.6, 55.6, 55.1, 12.2; HRMS (m/z) 396.1378 [M+H]⁺, calcd 396.1376 C₂₁H₂₂N₃O₃S⁺.

2.1.1.9 Synthesis of (*E*)-3-buten-2-one-4-(4-hydroxy-3-methoxyphenyl)-2-(4-(4-chlorophenyl)-2-thiazolyl)hydrazone (**9**)

Using the general procedure described above (section 2.1.1), **9** was obtained as an orange solid in 88 % yield. Mp: 166.2-166.8 °C; IR (cm⁻¹): 3487, 2964, 1616, 1591, 1513, 1489, 1280, 1257, 755; ¹H NMR (200 MHz, DMSO-d₆), δ/ppm: 11.1 (1H, s), 9.2 (1H, s), 7.9 (2H, d), 7.4 (1H, d), 7.3 (1H, d), 7.2 (1H, s), 6.98 (1H, d), 6.91 (1H, d), 6.7-6.6 (2H, m), 3.8 (3H, s), 2.1 (3H, s); ¹³C NRM (50 MHz, DMSO-d₆), δ/ppm: 169.7, 149.6, 149.2, 148.3, 147.6, 134.1, 132.8, 132.2, 128.9, 128.4, 127.6, 126.0, 121.1, 115.9, 110.4, 105.0, 50.0, 12.6; HRMS (m/z) 400.0881 [M+H]⁺, calcd 400.0881 C₂₀H₁₉ClN₃O₂S⁺.

2.1.1.10 Synthesis of (*E*)-2-[(2-(heptan-2-ylidene)hydrazo]-4-(4-cyanophenyl)-thiazole (**12**)

Using the general procedure described above (section 2.1.1), **12** was obtained as a pale solid in 46 % yield. Mp: 188.2-192.7 °C; ¹H NMR (200 MHz, CDCl₃), δ/ppm: 12.2 (1H, s), 7.8 (2H, d, *J* = 8.4 Hz), 7.7 (2H, d, *J* = 8.4 Hz), 7.0 (1H, s), 2.4 (2H, m), 2.2 (3H, m), 1.6 (2H, m), 1.3 (4H, m), 0.9 (3H, m); ¹³C NRM (50 MHz, CDCl₃), δ/ppm: 169.8, 163.5, 138.3, 133.2,

131.1, 126.1, 113.7, 104.3, 38.2, 31.1, 25.2, 22.2, 18.1, 13.8; HRMS (m/z) 313.1491 [M+H]⁺, calcd 313.1481 C₁₇H₂₁N₄S⁺.

2.1.1.11 Synthesis of (E)-4-(4-chlorophenyl)-2-[2-(1-(4-aminophenyl)ethylidene)hydrazinyl]-1,3- thiazole (13)

Using the general procedure described above (section 2.1.1), **13** was obtained as a brown solid in 85 % yield. Mp: 192.8-194.2 °C; ¹H NMR (200 MHz, Acetone-d₆), δ/ppm: 7.9 (2H, d), 7.6 (2H, d), 7.4 (2H, d), 7.2 (1H, s), 6.7 (2H, d), 2.4 (3H, s); HRMS (m/z) 343.0787 [M+H]⁺, calcd 343.0779 C₁₇H₁₆ClN₄S⁺.

2.1.1.12 Synthesis of (E)-2-[(2-benzylidenecyclohexylidene)hydrazinyl]-4-(cyanophenyl)thiazole (14)

Using the general procedure described above (section 2.1.1), **14** was obtained as a red solid in 72 % yield. Mp: 169.7-171.2 °C; ¹H NMR (200 MHz, DMSO-d₆), δ/ppm: 8.0 (2H, d), 7.8 (2H, d), 7.6 (1H, s), 7.4-7.2 (6H, m), 7.0 (1H, s), 2.6-2.5 (4H, m), 1.7-1.5 (4H, m); HRMS (m/z) 385.1490 [M+H]⁺, calcd 385.1481 C₂₃H₂₁N₄S⁺.

2.1.1.13 Synthesis of (E)-2-propenal-3-phenyl-2-[4-(4-chlorophenyl)2-thiazolyl]hydrazone (15)

Using the general procedure described above (section 2.1.1), **15** was obtained as a pink solid in 91 % yield. Mp: 194.8-196.6 °C; ¹H NMR (200 MHz, DMSO-d₆), δ/ppm: 8.1-8.0 (1H, dd), 7.9-7.8 (2H, d), 7.6 (1H, s), 7.7-7.5 (2H, m), 7.5-7.1 (7H, m), 7.1-6.9 (2H, m); HRMS (m/z) 340.0678 [M+H]⁺, calcd 340.0670 C₁₈H₁₅ClN₃S⁺.

2.2. Biological assay

2.2.1 Fungal strains and inoculum quantification

For the antifungal evaluation, the following strains from the American Type Culture Collection (ATCC, Rockville, MD, USA) were used: *Cryptococcus gattii* (ATCC32608), *C. neoformans* (ATCC24067), *Candida albicans* ATCC 18804, *C. krusei* (ATCC 20298), *C. parapsilosis* (ATCC 22019), *C. tropicalis* (ATCC 750) and *Paracoccidioides brasiliensis* (Pb18). All fungi strains were obtained from the fungi collection of the Faculty of Medicine of the Universidade de São Paulo (São Paulo, SP, Brazil). The fungi strains were maintained on Sabouraud Dextrose Agar (SDA, Oxoid, Basingstoke, UK) for most species, and YPD (Yeast, Peptone and Dextrose) for *P. brasiliensis*. All yeast strains were stored frozen at -80°C.

Final inocula for *Candida* and *Cryptococcus* species were of 1.5×10^3 CFU/mL and were prepared using the spectrophotometric dilution method. Broth microdilution testing was performed in accordance with the guidelines in the CLSI M27-A3 document [32], with modifications proposed by Johann et al. [33]. To inoculate the cultures of *P. brasiliensis* yeast cells were aseptically collected with a bacteriological loop and suspended in 5 mL of sterile saline solution 0.9%. The suspension was homogenized by vortexing for approximately 10 seconds. Suspensions containing larger aggregates of cells were rested before decantation, and then, only the supernatant was collected. The transmittance was measured at a wavelength of 530 nm and then adjusted to 70%, which corresponded to $1-5 \times 10^6$ cells/mL [34]. The resulting suspensions were diluted in RPMI medium supplemented with L-glutamine and buffered to pH 7.0 with 0.165 M morpholine propanesulfonic acid (MOPS) (Sigma, St Louis, USA), broth (1:10) to obtain a final inoculum with $1-5 \times 10^5$ yeasts/MI [35].

2.2.2 Determination of minimum inhibitory concentration (MIC)

Broth microdilution testing was performed in accordance with the guidelines in the CLSI document M27-A3 [32]. Susceptibility towards our test compounds was determined by the microbroth dilution method, which was performed in sterile flat-bottom 96-well microplates (Difco Laboratories, Detroit, MI, USA). The compounds were dissolved in DMSO (Vetec, RJ, Brazil) and diluted in synthetic RPMI medium to obtain a final concentration of 250 μ M. Compounds with activity at this concentration underwent a new test in to determine their potency (MIC values). The antifungal candidates were tested at concentrations of 0.45-250 μ M, with pure RPMI media as growth and sterile control. Fluconazole (0.125 a 64 μ g/mL), amphotericin B and itraconazole (0.03 a 16 μ g/mL) were included as the positive antifungal controls. After inoculation of fungal strains, the plates were incubated at 35 °C during 48 h for the *Candida* species, 72 h for *Cryptococcus* spp. and 7 days for *P. brasiliensis*. The endpoints were determined visually by comparison with the endpoints of the drug-free growth-control wells. All tests were performed in triplicate. The value of the minimum inhibitory concentration (MIC) was defined as the lowest compound concentration (μ M) at which the well was optically clear.

2.2.3 Cytotoxicity assay in human cells

Human non-tumor embryonic kidney HEK 293 cells were kindly provided by Dr. Marcel Leist, University of Konstanz / Germany. These cells were cultured in high glucose DMEM medium (Sigma Aldrich, USA) supplemented with both 10% fetal bovine serum (GIBCO BRL, Grand Island, NY) and 1% antibiotic solution (100 IU/mL penicillin and 100 μ g/mL streptomycin

(GIBCO BRL, Grand Island, NY). Cells were maintained in the logarithmic growth phase in incubator with 5% CO₂ at 37°C.

Cytotoxicity in HEK 293 cells was assessed by the MTT assay as described by Mosmann [36]. Briefly, HEK cells were plated at the density of 1×10^4 cells per well in 96-well plate and incubated overnight. After incubation, the cells were treated for 72 hours with thiazole derivatives, amphotericin B, fluconazole and itraconazole using seven serial dilutions between 250-0.016 μ M. Cell viability was evaluated by the rate of reduction of 3-(4,5-dimethylthiazol-2-yl) -2,5-diphenyltetrazolium bromide (MTT) to formazan crystals quantified by absorbance at 570 nm in a spectrophotometer (VersaMax). The IC₅₀ was calculated by non-linear regression using GraphPad Prism® Version 5.01 software (GraphPad Software Inc., La Jolla, CA, USA). The results were expressed as the percentage of viability in relation to the negative control (DMSO, 0.5%), which was calculated as follows: Percentage of cell viability (%) = [(treated mean OD / negative control) x100] and obtained with two independent experiments performed in triplicate.

2.3 Molecular modeling studies

2.3.1 Dataset compounds

Twenty-two compounds with *C. neoformans* minimum inhibitory concentration (MIC) were employed in the 2D- and 3D-QSAR studies. The dataset comprises thiazole derivatives retrieved from the literature [20], and those synthesized in this work. All dataset compounds were tested for antifungal activity using the same experimental conditions, allowing the construction of QSAR models due to the equivalence of biological data. MIC values were converted into pMIC (-LogMIC) for the inference of the statistical models.

Initially, 2D structures of the dataset compounds were constructed using Discovery Studio Visualizer [37] and the 3D lowest energy conformation was generated by OMEGA 2.5.1.4 [38,39]. After, all compounds were aligned in common scaffold (hydrazine-thiazole and benzene ring) using lowest energy conformation of the (*E*)-3-[2-(4-(4-methoxyphenyl)thiazol-2-yl)hydrazono]]butan-1-ol [20]. Dataset was separated into two subsets: a training set (80% of a total number of compounds) which was employed in the model inference and used for internal validation) and a test set (20% of the complete set) which was used for predictions and external validation. Three features were used for generating individual hierarchical cluster analysis (HCA): antifungal space (values of pMIC for *C. neoformans* inhibition), drug-like space (represented by molecular weight, ClogP, number of hydrogen bond donors and acceptors, fraction of sp³ carbons, and number of rotatable bonds), and 2D molecular similarity (represented by MACC fingerprints). All descriptors from drug-like and 2D similarity spaces were calculated with PaDEL-Descriptor [40]. HCA was performed

considering the incremental-linkage clustering method and the normalized Euclidian distance calculated between each pair. All HCA calculations were performed by using Chemoface software [41]. After clustering, 20% of compounds were randomly selected for each cluster of all three HCA, in order to ensure that training and test set compounds would remain representative of the total dataset considering its biological activity, physicochemical properties, and molecular structure.

2.3.2 Construction and validation of HQSAR model

After construction of the 3D molecular structure of dataset compounds and its rational division in training/test sets, hologram QSAR (HQSAR) models were generated in order to predict *C. neoformans* inhibitory activities. All HQSAR models were constructed using training set compounds and Sybyl X 2.1 package [42]. First, 32 HQSAR models were constructed using different combinations of fragment distinction parameters, which constitutes the parameters employed to generate the molecular hologram: atoms [A], bonds [B], connections [C], hydrogen atoms [H] and hydrogen bonds acceptor/donor [DA]. This initial screening employed fragment size fixed to contain 4 to 7 atoms. The three most robust HQSAR models (highest q^2 values among their pairs) were selected to test the influence of fragment size in statistical parameters. At that point, twenty-seven new HQSAR models were constructed by fixing the fragment distinction and then varying the fragment size as 1-4 atoms, 2-5 atoms, 3-6 atoms, 5-8 atoms, 6-9 atoms, 7-10 atoms, 8-11 atoms, 9-12 atoms and 10-13 atoms. In both stages of HQSAR model construction (fragment distinction and fragment size variation), models with different hologram lengths were generated (from 53 to 401 bins according to HQSAR default parameters).

2.3.3 Construction of 3D-QSAR models

Comparative Molecular Fields Analysis (CoMFA) and Comparative Molecular Similarity Index Analysis (CoMSIA) were employed as chosen 3D-QSARs approaches. Both studies were carried out with Sybyl X 2.1 package. Before 3D-QSAR studies, atomic charges were calculated with the PM3 method using MOPAC software implemented in Sybyl X 2.1 package. Then, CoMFA and CoMSIA models were first constructed using default parameters, which are energy cutoff set as 30 kcal/mol, a sp^3 carbon atom positively charged used as a probe and grid generated with 2 Å of distance between each grid point. In parallel, CoMSIA models were constructed from different combinations of similarity indexes (electrostatic, steric, hydrophobic, H-bond acceptor and H-bond donor fields). After construction of the first CoMFA and CoMSIA models, the region focusing technique was applied to select most relevant variables and to obtain more robust models: the distance between grid points was

varied from 0.5 to 3 Å and a standard deviation factor obtained from first models was applied to correct calculated fields.

2.3.4 Statistical Validations of 2D- and 3D-QSAR models

All HQSAR, CoMFA and CoMSIA models were evaluated according to i) internal validation coefficient calculated with leave-one-out method (q^2), ii) regression coefficient (r^2) and iii) its respective errors (standard error of validation [SEV] and standard error of estimation [SEE]). The three most robust models were selected for external validations with test set compounds and the following metrics were analyzed: i) external validation coefficient (r^2_{test}), ii) r^2_m , a coefficient for comparison between adjusted external validation coefficient and external validation coefficient forced to pass through the origin (r^2_0), r^2_m' , the same coefficient calculated with inverted axis and its iii) average ($avgr^2_m$) and iv) difference (Δr^2_m) [43], v) $Q^2_{(t2)}$ and vi) $Q^2_{(t3)}$ metrics, and vii) Concordance Correlation Coefficient (CCC) was employed for check the correlation between the precision (fitting of observed data with fitting line) and accuracy (how deviated the regression line is the slope 1 when intercepting origin point) [44]. Error metrics as RMSEP and MAE were also evaluated as external validations.

The most predictive HQSAR, CoMFA and CoMSIA models were submitted to leave-N-out internal validation, where N size ranged from 5 to 20 groups of compounds. The compounds of each N sized group were randomly selected by the validation algorithm and to disregard the bias, the validation was performed in triplicate. Twenty runs of progressive-scrambling validations were also performed to the most predictive models to verify chance correlation of the constructed model. Progressive-scrambling is similar to the Y-scrambling procedure but performs a scrambling of pMIC values in different activities ranges. In this work, we selected 2 distinct ranges of pMIC (complete dataset and a dataset divided into two groups according to average pMIC values [called 50/50 subset]) to generate 10 scrambled models for each subset division. Then, models generated with scrambled activities of 50/50 subset would produce better validation metrics than full scrambled models [45].

2.3.5 Construction and validation of similarity models

In addition to QSAR models, we constructed 3D similarity models for classification of the studied dataset into active/inactive classes. Five compounds with highest MIC values were labeled as active, while the other compounds were considered inactive. Furthermore, 50 decoys (putative inactive compounds) were generated for each active compound using DUD-E web-server [46]. Then, vROCS software [47,48] was employed to construct and validate chemical similarity models. Initially, ROCS models were constructed considering all

chemical features of template compounds, which was followed by a screening of feature exclusion and weight applying was performed aiming to verify the predictability of models. After construction of models, 30 conformers of dataset compounds (active, inactive and decoys) were generated with OMEGA software and models were applied to rank substances according to similarities, evaluated by shape (volume) and color (chemical features: ring, hydrogen bond acceptor and donor, a hydrophobic group, ionizable groups). Similarity was ranked by the values of TanimotoCombo coefficient [TCcombo], which is a sum of Tanimoto coefficient for shape and color). Additionally, the area under the curve (AUC) and enrichment factor values were calculated to infer the ability to discriminate active from inactive compounds. Similarity models were also evaluated by the so-called confusion matrix, which considers the number of true positives and negatives [TP and TR] and false positives and negatives [FP and FR] classifications, together with the true positive and true negative rates (TPR and TNR, respectively) themselves, accuracy (sum of true positive and true negative classifications divided by total number of dataset compounds), F1 score and Matthews correlation coefficient (MCC) as illustrated by equations 1 and 2, respectively [43].

$$F1\ score = \frac{2TP}{2TP + FP + FN} \quad (\text{Eq. 1})$$

$$MCC = \frac{TP \times TN - FP \times FN}{\sqrt{(TP + FP)(TP + FN)(TN + FP)(TN + FN)}} \quad (\text{Eq. 2})$$

2.3.6 External blind validation of QSAR and similarity models

At final of molecular modeling studies, a second external validation was carried using compounds **10-15** for QSAR models and for ROCS model, denominated blind set. **Figure 1** presents a flowchart of current work highlighting experimental approaches in blue squares and computational ones in red squares.

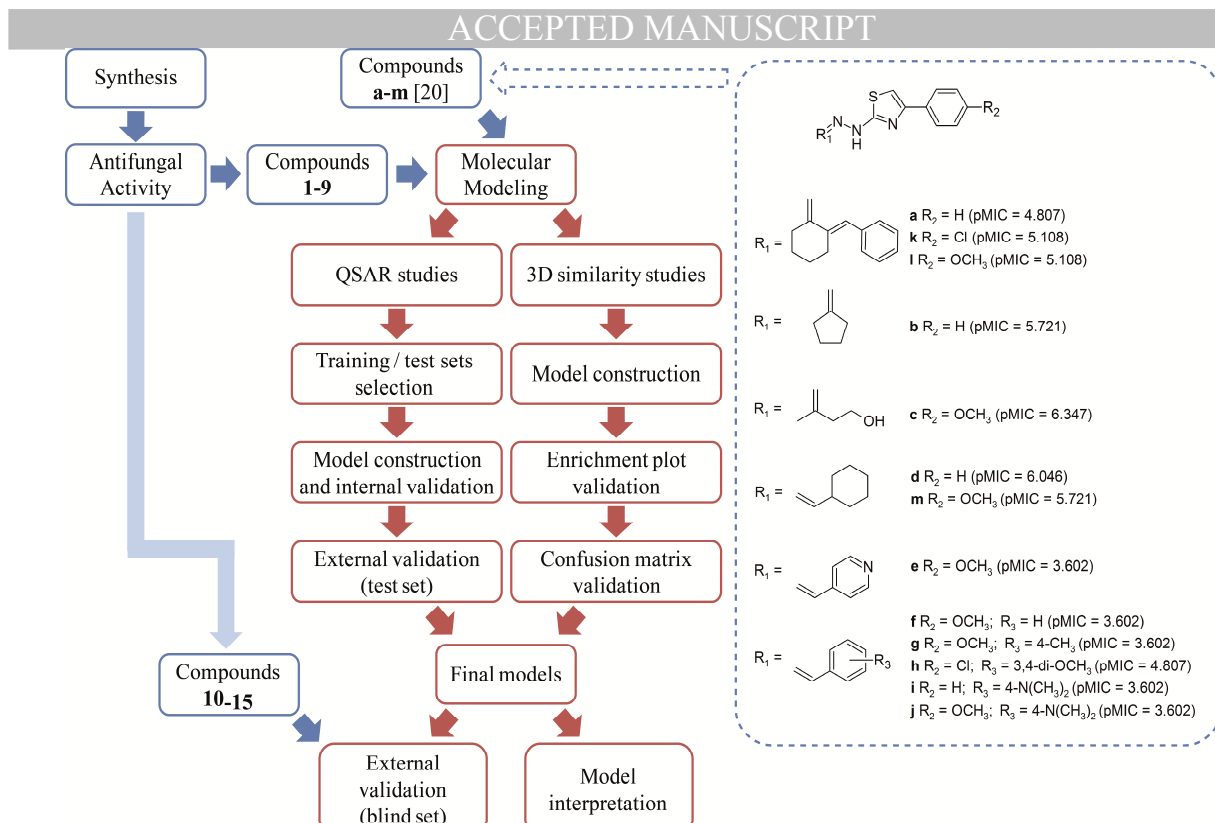


Figure 1. Experimental and computational workflow. Structure and pMIC values for *C. neoformans* inhibition of compounds **a-m** [20].

3. Results and discussion

3.1 Chemistry

The hydrazine-thiazole derivatives **1-15** (**Figure 2**) were synthesized using a classical method as previously reported [31] and briefly described below.

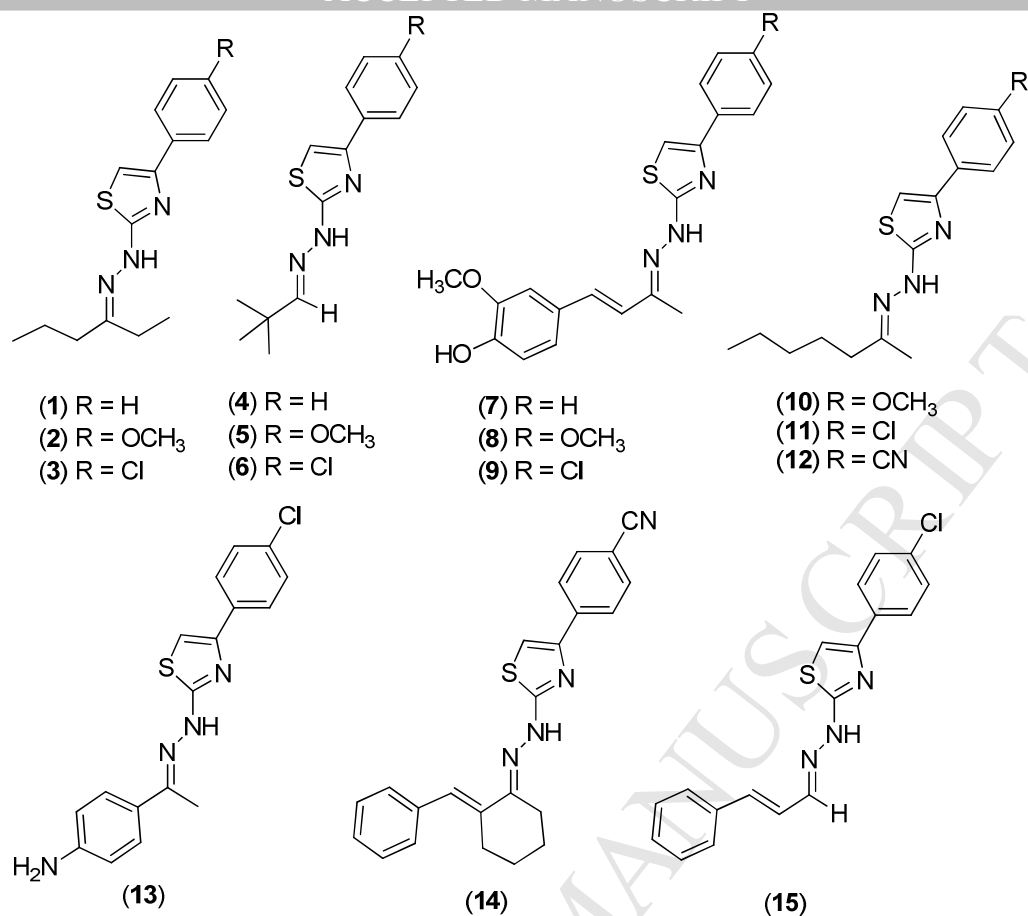
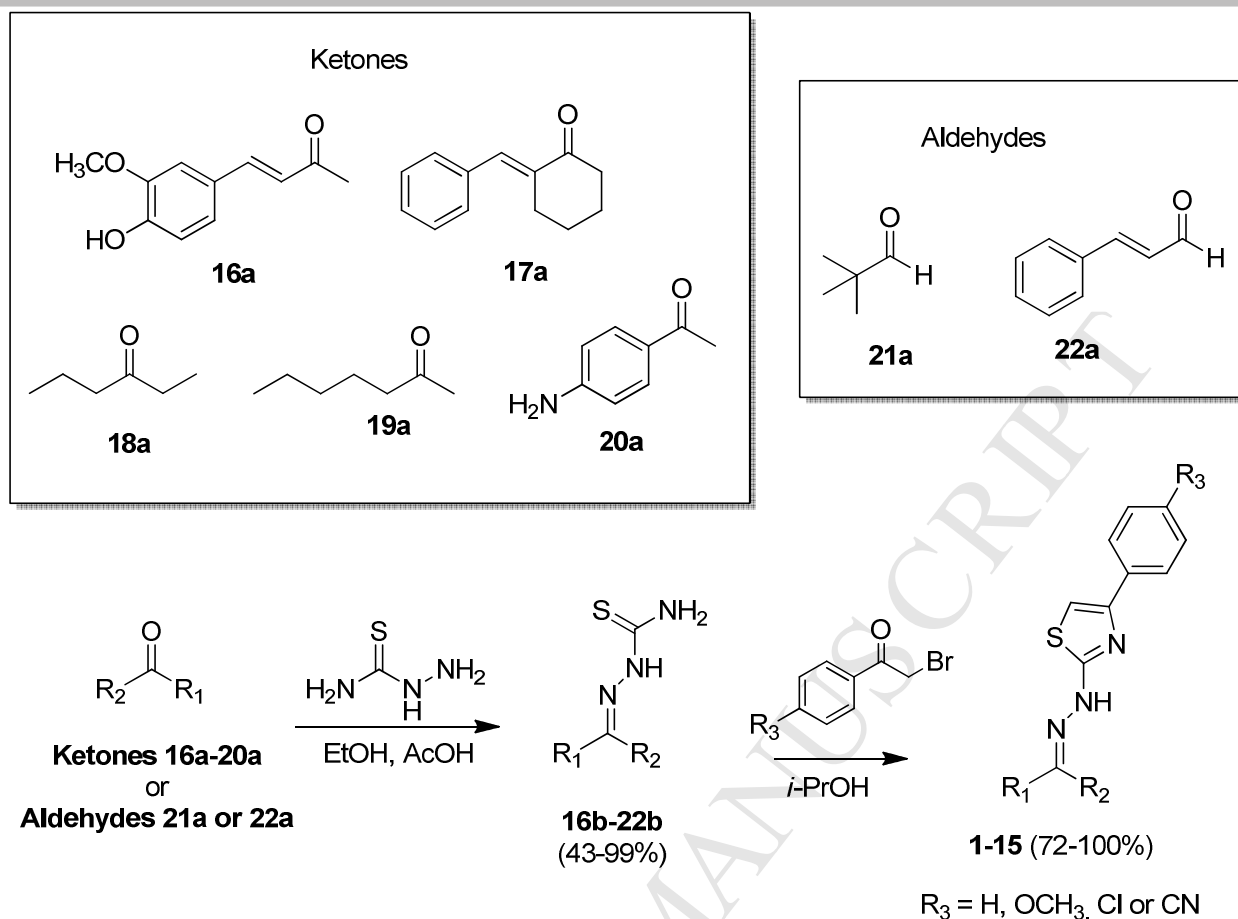


Figure 2 - Chemical structure of the hydrazine-thiazoles synthesized.

The ketones **16a** and **17a** were prepared by crossed aldol condensation between acetone and 4-hydroxy-3-methoxybenzaldehyde or cyclohexanone and benzaldehyde in acidic and basic conditions, respectively. Reaction of the ketones or the aldehydes with thiosemicarbazide under acidic conditions, gave the corresponding thiosemicarbazones **16b-22b**, which were cyclized with α -bromoacetophenone to yield the thiazole heterocycles **1-15** (Scheme 1).



Scheme 1 - General scheme for the preparation of hydrazine-thiazoles **1-15**

All thiosemicarbazones had already been described and their melting point and spectroscopic data are in accordance with the reported values in literature. The structures of the novel hydrazine-thiazoles **1-15** were confirmed by spectroscopic methods and high-resolution mass spectra. The ^1H and ^{13}C NMR data confirmed the formation of the thiazole moiety by presence of a signal at around 7.0 ppm and 104.0 ppm, which corresponds to the methine proton and carbon, respectively, of the thiazole ring. The hydrazine-thiazoles **1-3** were obtained as 1:1 mixture of *E* and *Z* isomers (C=N double bond), determined according to ^1H NMR signal integration of N-H at ~ 13.8 and 12.4 ppm. According to Tenchiu *et al.* (2009), the signal assigned to N-H “appears at 9-12 ppm for the *E*-form, and 14-15 ppm for the *Z*-form” [49]. In all other cases, (*E*)-isomers were obtained predominantly, as evidenced by ^1H NMR spectroscopic data and compared with similar structures [50].

3.2 Biological assays

All the hydrazine-thiazoles and the thiosemicarbazones **16b**, **18b** and **21b** were tested for *in vitro* antifungal activity against seven clinically important fungal species, namely *Candida albicans*, *C. krusei*, *C. parapsilosis*, *C. tropicalis*, *Cryptococcus neoformans*, *C. gatti* and

Paracoccidioides brasiliensis. Some thiosemicarbazones were included for comparison purposes. The minimum inhibitory concentration (MIC) values are shown in **Table 1**.

Table 1 – Minimum inhibitory concentration (MIC) in μM of synthesized compounds

Compound	<i>C. albicans</i>	<i>C. krusei</i>	<i>C. parapsilosis</i>	<i>C. tropicalis</i>	<i>C. gatti</i>	<i>C. neoformans</i>	<i>P. brasiliensis</i>
18b	>250	>250	>250	>250	>250	>250	>250
1	3.9	3.9	15.6	3.9	3.9	3.9	250
2	3.9	7.8	15.6	7.8	1.9	3.9	62.5
3	0.9	1.9	1.9	3.9	0.45	0.9	250
21b	>250	>250	>250	>250	>250	>250	>250
4	3.9	5.8	3.9	31.2	1.9	1.9	125
5	3.9	7.8	3.9	31.2	0.9	1.9	250
6	1.9	2.9	3.9	250	0.9	1.9	125
16b	>250	>250	>250	>250	>250	>250	>250
7	250	250	250	250	250	250	250
8	250	250	250	250	250	250	ND
9	250	250	250	250	125	250	62.5
10	ND	ND	ND	ND	0.76	1.5	>250
11	1.5	1.5	24.2	5.9	0.75	0.75	>250
12	31.2	15.6	125	250	3.9	3.9	250
13	>250	>250	>250	>250	>250	>250	>250
14	>250	>250	>250	>250	81.2	20.3	>250
15	>250	>250	>250	>250	>250	>250	>250
Fluconazole	1.6	104.4	3.2	6.5	12.7	6.2	ND
Amphotericin B	0.3	0.5	0.5	1.2	0.08	0.09	0.06
Itraconazole	0.7	0.18	0.18	0.09	0.18	0.04	0.06

ND = not determined

From the obtained results, it can be concluded that the presence of the thiazole ring was essential for the activity since the corresponding thiosemicarbazones **16b**, **18b** and **21b** that lacks such ring were inactive. It is possible to infer also that the presence of a hydrophobic aliphatic chain plays a very important role in the antifungal activity. Since, the most promising compounds **1-6** and **10-12** have an aliphatic substituent in the hydrazine moiety. In general, the presence of the chlorine substituent in aromatic ring (R_3 in **Scheme 1**) was shown to increase activity with regard to all fungal species tested (**1, 2 vs 3** and **4, 5 vs 6**), except for *C. tropicalis* and *P. brasiliensis*. The active hydrazine-thiazoles showed a broad spectrum of

action against several pathogenic fungi, some of them being equally or more active than the positive controls fluconazole and amphotericin B. It is worth mentioning that compound **3** showed more activity than fluconazole against all fungal strains. Compounds **10** and **11** were the most potent against *C. neoformans* and *C. gattii* and are therefore very promising antifungal candidates. The antifungal activity of compound **10** against various clinical fungal isolates of *Candida* spp. has previously been described by Carradori et al. (MIC = 2-32 $\mu\text{g/mL}$) [26] and therefore this compound was not tested against *Candida* spp. in the present work. None of the compounds was sufficiently active against *P. brasiliensis*.

The results obtained in our studies are in accordance with those obtained by other authors that also reported the anti-*Candida* activity of hydrazine-thiazoles with hydrophobic features [26,51,52]. However, to the best of our knowledge, the activity of this class of molecules against *Cryptococcus* species is still very little studied. The mechanism of action of this class of compounds has not yet been fully elucidated. However, recently, our research group has shown that the activity of these thiazoles can be related to an increase in intracellular reactive oxygen species (ROS) such as superoxide, causing oxidative stress in the fungal cells [53].

In addition, the cytotoxicity of the active compounds was evaluated in human embryonic kidney (HEK-293) cells and the results are shown in **Table 2**. All compounds displayed low cytotoxicity toward human cells with IC_{50} values higher than at least 50 μM . These results demonstrate the enormous potential of these hydrazine-thiazoles with regard to both antifungal activity and selectivity.

Tabela 2 - Cytotoxicity of compounds on HEK cells

Compounds	IC_{50} (μM)	% viability at highest concentration tested
1	> 250*	52.41 \pm 6.58
2	207.00 \pm 12.89	-
3	237.86 \pm 9.71	-
5	> 50*	94.86 \pm 6.96
6	> 50*	94.96 \pm 7.22
10	> 250*	76.23 \pm 7.40
11	> 250*	66.10 \pm 6.00
12	184.69 \pm 13.72	-
14	> 50*	87.65 \pm 7.83
Amphotericin B	78.62 \pm 10.93	-
Fluconazole	> 250*	99.21 \pm 6.04
Itraconazole	> 250*	90.76 \pm 6.47

*Highest concentration tested based on the solubility of the compound in the assay medium. Data are presented as mean \pm standard deviation obtained from three independent experiments performed in triplicate. Itraconazole and Fluconazole data were obtained from two experiments.

3.3 Molecular modeling studies

3.3.1 QSAR Studies

Initially, the dataset division into training and test set was achieved its main goal: to distribute training and test set compounds homogeneously according to its biological, structural and chemical spaces. Supplementary Figure S1 illustrates that both training and test set compounds are distributed in the same proportion of complete dataset compounds in each observed cluster of all three analyzed spaces. Therefore, the selected test set compounds were suitable to perform external validations procedures. The molecular alignment was also achieved with success since all hydrazine-thiazole scaffold and benzene rings are perfectly aligned (Supplementary Figure S2).

Using selected training set compounds, the first 16 HQSAR models were constructed using *C. neoformans* pMIC values by varying the fragment distinction and fixing the fragment size parameters. The two most robust HQSAR models considered atoms, connections, and presence of H-bond acceptors/donors ($q^2 = 0.792$) and atoms, bonds, connections and presence of H-bond acceptors/donors ($q^2 = 0.757$). Then, these two models were employed to fragment size variation originating 18 other models. The fragment size variation indicated that larger fragments have better correlation with biological activity (in this case, the most robust model has a q^2 equal to 0.877). All HQSAR models information is available at Supplementary Table S1 and the five most robust models which were submitted to external validations are shown in **Table 3**.

Table 3 - Five most robust HQSAR models using fragment size equals to 4 to 7 atoms.

No.	Fsize	Fdist	q^2	SEV	r^2	SEE	HL	PC
23	8_11	A/C/DA	0.854	0.439	0.966	0.210	61	4
25	10_13	A/C/DA	0.828	0.476	0.972	0.193	61	4
31	7_10	A/B/C/DA	0.860	0.429	0.974	0.187	97	4
32	8_11	A/B/C/DA	0.877	0.403	0.975	0.181	59	4
34	10_13	A/B/C/DA	0.834	0.468	0.963	0.221	83	4

Fsize: fragment size (number of atoms); Fdist: fragment distinction; q^2 : leave-one-out internal validation coefficient; SEV: standard error of validation; r^2 : calibration coefficient; SEE: standard error of estimation; HL: hologram length (bins); PC: number of PLS principal components.

Then, a standard CoMFA model was generated obtaining in an unsatisfactory result ($q^2 = 0.531$). Therefore, we applied the region focusing strategy in order to improve the robustness of CoMFA models. From all 28 generated CoMFA models, eighteen models presented acceptable robustness ($q^2 > 0.6$) and the five most robust were generated using the original distance between grid points (2Å). The five most robust models (**Table 4**) indicate that steric effects have higher contribution than electrostatic one, indicating that van der Waals effects could be slightly more important to antifungal activity of studied series. This result corroborates SAR studies presented in this work and presented in previous work reporting

part of dataset compounds [20]. Models reported in **Table 4** were also submitted to external validations.

Table 4 - Five most robust CoMFA models using region focusing technique.

Model	W	d	q^2	SEV	PC	r^2	SEE	S	E
6	0.5	1	0.741	0.604	4	0.979	0.174	0.521	0.479
9	0.7	1	0.758	0.584	4	0.979	0.173	0.528	0.472
12	0.9	1	0.762	0.579	4	0.980	0.168	0.553	0.447
15	1.1	1	0.752	0.592	4	0.980	0.169	0.589	0.411
18	1.2	1	0.744	0.601	4	0.979	0.173	0.611	0.389

w: weight factor based on standard deviation; d: distance factor applied on distance of grid points; q^2 : leave-one-out internal validation coefficient; SEV: standard error of validation; r^2 : calibration coefficient; SEE: standard error of estimation; S: fraction of steric contribution to model; E: fraction of electrostatic contribution to model; PC: number of PLS principal components

After HQSAR and CoMFA model construction, 31 standard CoMSIA models were generated by combining similarities indexes (steric, electrostatic, hydrophobic, H-bond acceptor and donor). In this step, only one model constructed using H-bond donor (D) similarity index presented acceptable q^2 value (equal to 0.702). In addition, a second most robust model (electrostatic/donor, $q^2 = 0.656$) was also selected to region focusing technique. In total, 85 CoMSIA models were constructed and compared according to their robustness (Supplementary Table S3 and S4). From this analysis, five most robust CoMSIA models were selected and submitted to external validations (**Table 5**). All top five CoMSIA models were generated using both H-bond donor (D) and electrostatic indexes and, in all cases, D presented a minor contribution to models, indicating the importance of electrostatic interactions to explain the antifungal activity.

Table 5 - Five most robust CoMSIA models using region focusing technique.

Model	W	d	q^2	SEV	PC	r^2	SEE	D	E
66	0.5	1.5	0.843	0.471	4	0.937	0.298	0.193	0.807
69	0.7	1.5	0.866	0.435	4	0.947	0.275	0.181	0.819
72	0.9	1.5	0.883	0.406	4	0.945	0.278	0.185	0.815
75	1.1	1.5	0.876	0.419	4	0.939	0.293	0.184	0.816
78	1.2	1.5	0.869	0.429	3	0.936	0.301	0.182	0.818

w: weight factor based on standard deviation; d: distance factor applied on distance of grid points; q^2 : leave-one-out internal validation coefficient; SEV: standard error of validation; r^2 : calibration coefficient; SEE: standard error of estimation; **D: fraction of H-bond donor contribution to model**; E: fraction of electrostatic contribution to model; PC: number of PLS principal components.

After generation and comparison of robustness of 2D- and 3D- QSAR models, top five most robust models were submitted to external validations in order to select the most predictive model of each technique to continue QSAR studies. Then, models HQSAR 23, CoMFA 6 and

CoMSIA 75 showed higher $Q_{2(F1)}$, $Q_{2(F2)}$, $Q_{2(F3)}$, r_m^2 metrics and CCC values than other models as well as lower error metrics values (RMSEP and MAE) (Table 6).

Table 6 - Comparison of external validation metric for top 5 most robust models generated with each QSAR technique.

Model	HQ SAR					CoMFA					CoMSIA				
	23	25	31	32	34	6	9	12	15	18	66	69	72	75	78
$Q_{(F1)}^2$	0.957	0.930	0.928	0.927	0.938	0.871	0.855	0.855	0.854	0.853	0.756	0.823	0.865	0.880	0.880
$Q_{(F2)}^2$	0.954	0.925	0.923	0.922	0.934	0.863	0.845	0.845	0.844	0.843	0.740	0.811	0.856	0.872	0.872
$Q_{(F3)}^2$	0.959	0.934	0.932	0.931	0.941	0.879	0.863	0.863	0.862	0.861	0.770	0.833	0.872	0.887	0.887
r_m^2	0.945	0.911	0.889	0.853	0.965	0.714	0.697	0.681	0.632	0.620	0.725	0.789	0.824	0.832	0.827
$r_m'^2$	0.931	0.916	0.938	0.902	0.933	0.841	0.821	0.810	0.797	0.790	0.839	0.877	0.905	0.919	0.913
Δr_m^2	0.014	0.005	0.049	0.049	0.032	0.127	0.124	0.128	0.164	0.170	0.114	0.088	0.080	0.087	0.087
AVGr r_m^2	0.938	0.913	0.913	0.878	0.949	0.777	0.759	0.745	0.714	0.705	0.782	0.833	0.865	0.875	0.870
CCC	0.977	0.962	0.960	0.957	0.967	0.926	0.916	0.914	0.913	0.911	0.874	0.908	0.929	0.937	0.937
RMSEP	0.203	0.259	0.262	0.265	0.244	0.352	0.373	0.374	0.375	0.375	0.484	0.412	0.360	0.340	0.339
MAE	0.181	0.219	0.232	0.234	0.201	0.237	0.297	0.307	0.317	0.321	0.393	0.318	0.269	0.241	0.232

$Q_{(F1)}^2$: predictive R^2 ; $Q_{(F2)}^2$: Schüürmann et al. q^2 ; $Q_{(F3)}^2$: Consonni et al. q^2 ; r_m^2 : Roy parameter to assess predictive power; $r_m'^2$: predictive power calculate with inverted axis; Δr_m^2 : $r_m^2 - r_m'^2$; AVGr r_m^2 : average r_m^2 value; CCC: concordance correlation coefficient; RMSEP: root mean squared error of prediction for test set; MAE: mean absolute error.

Then, these metrics reflect the predictive power of model and its capacity to predict the biological activity of compounds out of pMIC range employed in this study. Therefore, the most predictive models were submitted to leave-N-out cross-validation and progressive-scrambling as last validations. Those final validations indicated that both models were not obtained by chance (scrambled models q^2 lower than original model standard error of validation higher than original model), and models are consistent under training set variations (all leave-N-out validations coefficients were higher than 0.6) and did not show residual values higher than 1 logarithmic unit (Figure 3).

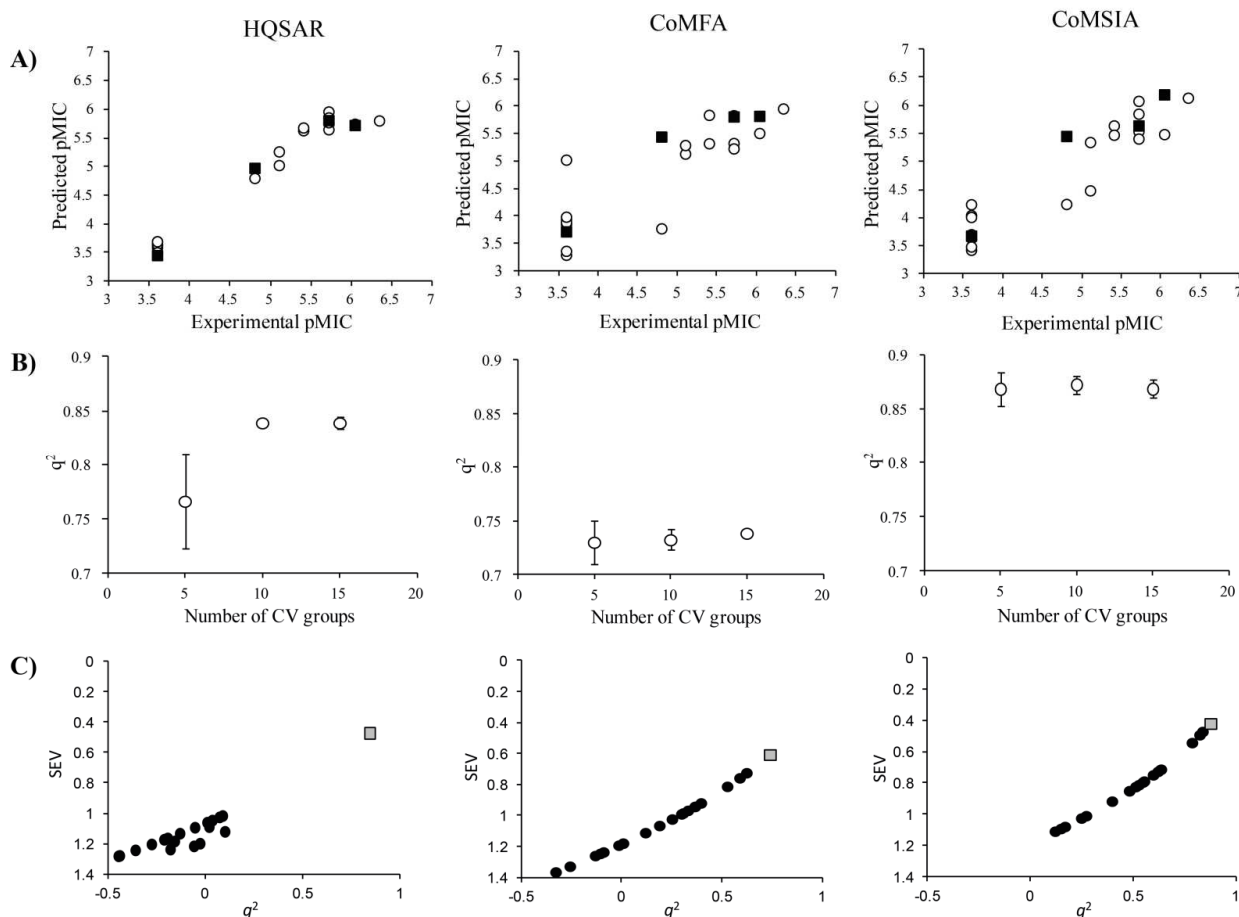


Figure 3 - Experimental versus predicted pMIC values (A, training set compounds are presented in white circles and test set compounds are presented in black square), leave-N-out internal validation (B) and progressive-scrambling (C, grey square represents original model and black circles represent scrambled models) and residual values for test set compounds.

Finally, validated models were employed to predict pMIC values for a blind set of compounds (Table 7). A comparison between residual values of test set and blind set indicated that 2D QSAR model outperform 3D ones in prediction of pMIC for compounds 10-15. We also estimated the applicability domain of generated QSAR models by analyzing the percentage of missing fragments (for HQSAR model) and the percentage of extrapolated variables (for CoMFA and CoMSIA models) of external validation set compounds in relation to training set compounds. This analysis demonstrate how test and blind set compounds are similar to training set ones according to their respective chemical spaces used to construct QSAR models: structural similarity for HQSAR, steric and electrostatic fields similarity for CoMFA, and electrostatic and H-bond donor similarity for CoMSIA. We concluded that high errors of prediction for blind set compounds (in special for compounds 13-15) could be associated with the fact of blind set compounds are far from applicability domain than test set ones for CoMFA and CoMSIA models.

Table 7 - Internal and external (using blind set) validations for top10 ROCS models.

cpds	HQ SAR				CoMFA			CoMSIA		
	exp. ^a	pred. ^b	res. ^c	% miss. ^d	pred. ^b	res. ^c	% miss. ^e	pred. ^b	res. ^c	% miss. ^e
test set										
1a	4.807	4.969	-0.162	0.00	5.456	-0.649	3.25	5.459	-0.652	6.27
1d	6.046	5.716	0.330	0.00	5.832	0.214	25.26	6.199	-0.154	10.36
4	5.721	5.800	-0.079	0.00	5.822	-0.101	2.28	5.646	0.075	5.06
7	3.602	3.447	0.155	0.00	3.731	-0.129	3.83	3.685	-0.083	2.41
blind set										
10	5.824	5.294	0.530	0.00	5.371	0.453	14.60	6.282	-0.458	28.19
11	6.125	5.284	0.841	1.00	5.715	0.410	10.99	6.398	-0.273	26.27
12	5.409	5.177	0.232	9.00	5.768	-0.359	25.05	6.336	-0.927	29.64
13	3.602	4.438	-0.836	8.00	5.172	-1.570	31.00	6.188	-2.586	15.90
14	3.788	4.901	-1.113	5.00	5.171	-1.384	30.02	4.270	-0.482	34.94
15	3.602	3.931	-0.329	0.00	4.847	-1.245	22.31	6.282	-2.463	32.53

^aexperimental pMIC values; ^bpredicted pMIC values; ^cresidual of prediction (a-b); ^dpercentage of missing fragments (HQ SAR) of external validation compounds in relation to training set ones; ^epercentage of extrapolated terms from grid points (CoMFA and CoMSIA) of external validation compounds in relation to training set ones.

From HQ SAR contribution maps (**Figure 4**), the hydrazine-thiazole group and the benzene attached to it as well as an aliphatic substituent of N-R region presented green, blue-green and yellow contributions, indicating that these groups are important to antifungal activity. In contrast, an aromatic ring of compound **f** located at the hydrophobic region is colored in red and orange, indicating that aromatic substituent at this region would contribute negatively to antifungal activity.

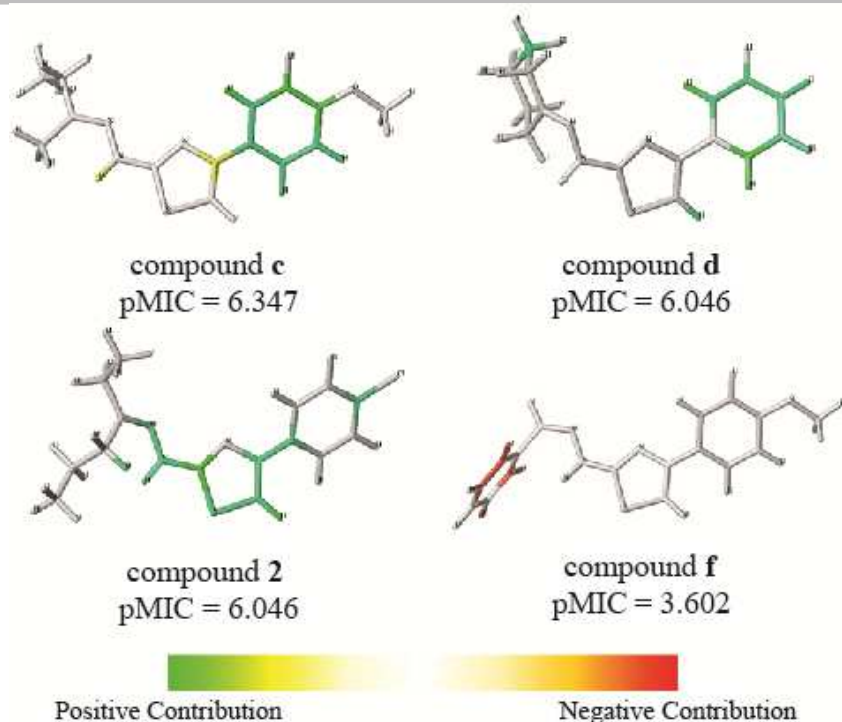


Figure 4 - Contribution maps generated with the best HQSAR model.

From CoMFA maps (**Figure 5**), both substituents at hydrazine group of most active compounds (**c** and **2**) are located at steric favored regions and pyridine ring of compound **e** is located at a steric impeachment region. Interestingly, the N atom of pyridine ring of compound **e** could form electrostatic interactions compensating the disfavored bulky region of this compound. Also, there is a very small green polyhedral located at methoxy substituent of benzene indicating that bulky groups at these regions could be slightly more active than others. There is a negatively charged favored region located near the three N atoms of thiazole ring and hydrazine group indicating that electron lone pairs could form an electrostatic interaction with its molecular target. Furthermore, there is a positively charged region located at hydroxyl group of hydrazine substituent of compound **c**.

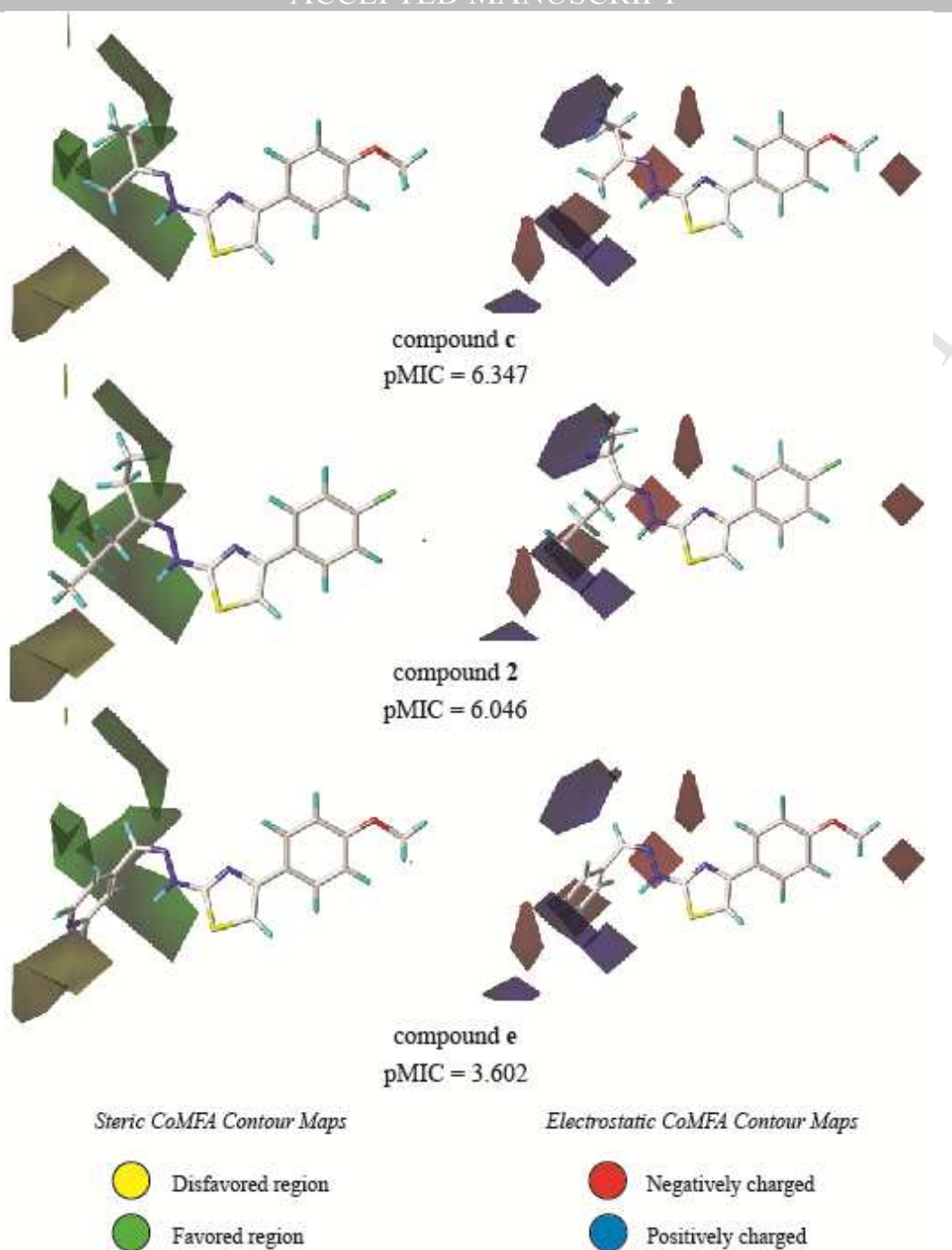


Figure 5 - Contour maps generated with best CoMFA model

Electrostatic CoMSIA contour maps (**Figure 6**) corroborates the CoMFA results, with one exception, the negative similarity region is located only at N atom of hydrazine group. Then, this finding plus the higher contribution of electrostatic similarity index for CoMSIA model could indicate the major contribution of hydrazine group to electrostatic interactions than thiazole ring. Finally, NH of hydrazine group is located at a favored H-bond donor region indicating the importance of an H-bond to biological activity.

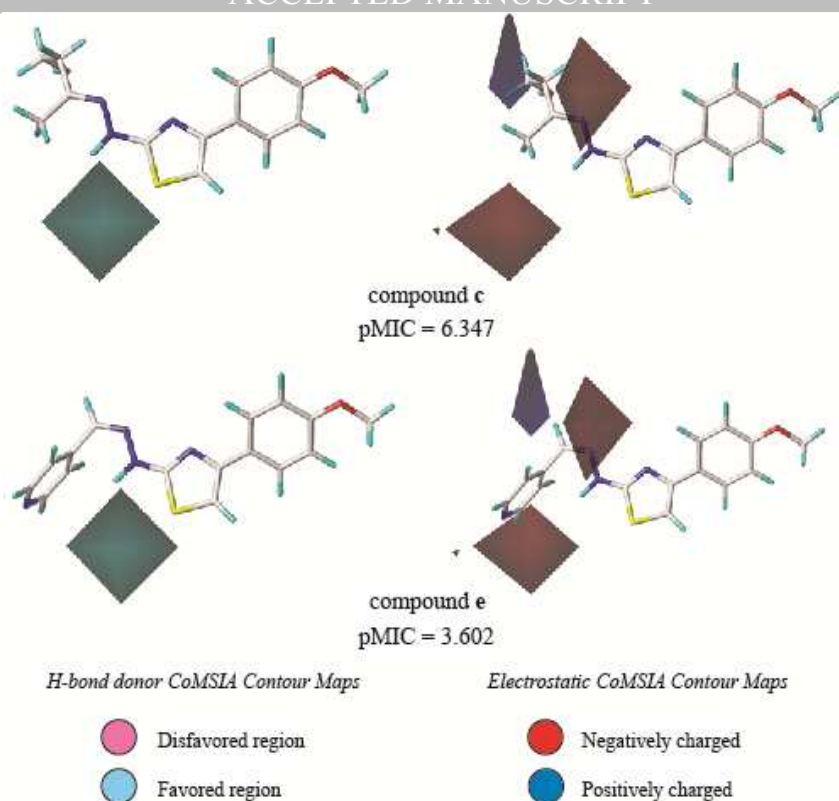


Figure 6 - Contour maps generated with best CoMSIA model.

3.3.2. Molecular Similarity Studies

Initially, five active compounds were employed to construct 15 models based on 3D molecular shape, chemical features and the sum of both. The AUC values ranged from 0.736 to 0.987, with no statistical difference between models: all confidence levels of AUC values were superimposed. Then, 74 new models were constructed by applying weight to each of the chemical features, by excluding chemical features or by the combination of both strategies. In this step, we did not use compound **i** due to lowest AUC values presented by models where it was employed as a template. This strategy allowed us to evaluate the importance of the individual chemical groups to the classification of compounds in active and inactive. All the 89 generated similarity models are reported in Supplementary Table S5.

All 89 generated similarity models were reported in Supplementary Table S5. Then, we selected 10 models with highest AUC values to validate it by a confusion matrix construction and calculation of classification metrics. In this step, we calculated the similarity between all dataset compounds with a query model and defined a cutoff value of TCcombo (to classify compounds in active or inactive) according to the first decoy found in the ranking. **Table 8** displays calculated results.

Table 8 - Internal and external (using blind set) validations for top10 ROCS models.

	Models										
	72	53	24	14	52	70	16	84	60	18	76
AUC	0.988	0.988	0.987	0.987	0.986	0.986	0.986	0.985	0.984	0.984	0.984
- 95% c.l. ^a	0.982	0.975	0.981	0.982	0.977	0.981	0.979	0.977	0.971	0.971	0.947
+ 95% c.l. ^b	1.000	1.000	1.000	1.000	1.000	1.000	1.000	1.000	1.000	1.000	1.000
EF 0.5% ^c	95.58	44.29	118.92	97.32	95.19	94.97	88.81	82.09	82.87	71.69	62.67
TCcombo cut-off	0.911	1.250	1.172	0.902	1.144	0.911	1.135	1.212	1.397	1.133	1.161
TPR	1.000	1.000	1.000	1.000	1.000	1.000	1.000	1.000	1.000	1.000	1.000
TNR	0.974	0.974	0.956	0.974	0.956	0.974	0.956	0.970	0.967	0.956	0.959
ACC	0.975	0.975	0.956	0.975	0.956	0.975	0.956	0.971	0.967	0.956	0.960
MCC	0.637	0.637	0.530	0.637	0.530	0.637	0.530	0.611	0.588	0.530	0.548
F1	0.588	0.588	0.455	0.588	0.455	0.588	0.455	0.556	0.526	0.455	0.476
TPR _{ext}	1.000	1.000	1.000	1.000	1.000	1.000	1.000	1.000	0.500	1.000	1.000
TNR _{ext}	0.000	0.750	0.000	0.000	0.000	0.000	0.000	0.750	0.750	0.000	0.250
ACC _{ext}	0.333	0.833	0.333	0.333	0.333	0.333	0.333	0.833	0.667	0.333	0.500
MCC _{ext}	0.000	0.612	0.000	0.000	0.000	0.000	0.000	0.612	0.250	0.000	0.158
F1 _{ext}	0.500	0.800	0.500	0.500	0.500	0.500	0.500	0.800	0.500	0.500	0.571

^{a, b} = lower and upper confidence levels values of AUC calculated with bootstrap validation, respectively; ^c = enrichment factor (actives found / decoys found) at 0.5% of entire database; _{ext} = metrics calculated with blind external validation set

Comparison of values of the confusion matrix shows no statistical differences among the ten most robust models. Then, the external validation using compounds **10-15** was fundamental to distinguish models due its capacity of to classify compounds according to active and inactive. Only models 53, 84 and 60 (**Figure 8B-D**) presented acceptable values of accuracy (> 60%), while all other seven models could be considered worse than a random model, due to low ACC values for external validation set (< 0.5). Another important observed characteristic of those top three models is that they have the highest TC-combo values defined as cutoff. This result indicates that active compounds of external validation set are more similar to model template. From top three models, model 84 is the first one to find all active molecules at ROC curve (**Figure 8A**). Altogether, these findings indicate the importance of hydrophobic feature as hydrozone substituent. For all selected models, the benzene and thiazole rings as well as hydrazone moiety has same features, indicating that these groups are important to antifungal activity.

Among the best three models, model 53 has a methoxyl substituent at the benzene ring, which when exploited during the ROCS model generation lead to more discriminant models, if an H-bond acceptor feature was included. This finding could indicate that this region could not directly interact with possible molecular targets and that only its shape influences the biological activity.

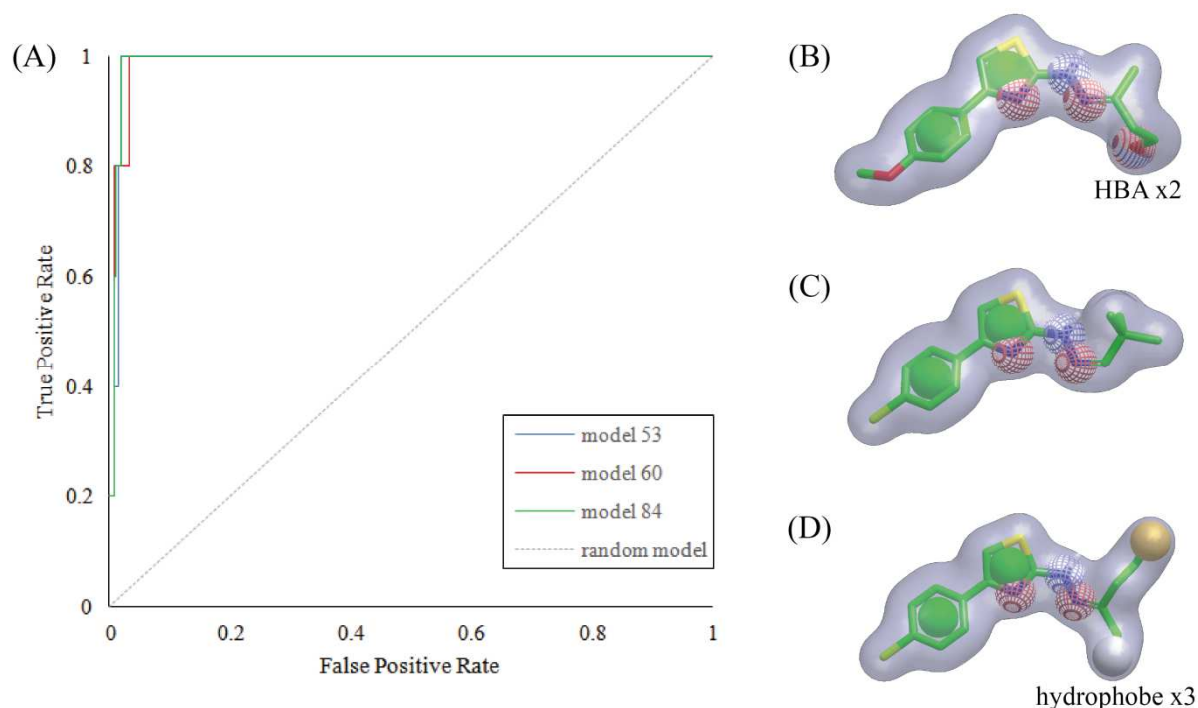


Figure 8 - (A) ROC curve of 3 best models and visual representation of model 53 (B), model 60 (C) and model 84 (D). Molecular features of models are presented as green spheres (rings), red spheres (H-bond acceptors), blue spheres (H-bond donors) and yellow/white spheres (hydrophobic groups).

From all molecular modeling studies (2D- and 3D-QSAR models as well as similarity models), several features were observed and showed importance to antifungal activity. In other words, those groups showed mathematical importance to pMIC prediction (or classification) and could be related to interactions with possible molecular targets. A brief summary of observed structure-activity relationship from molecular modeling studies is shown in **Figure 9**.

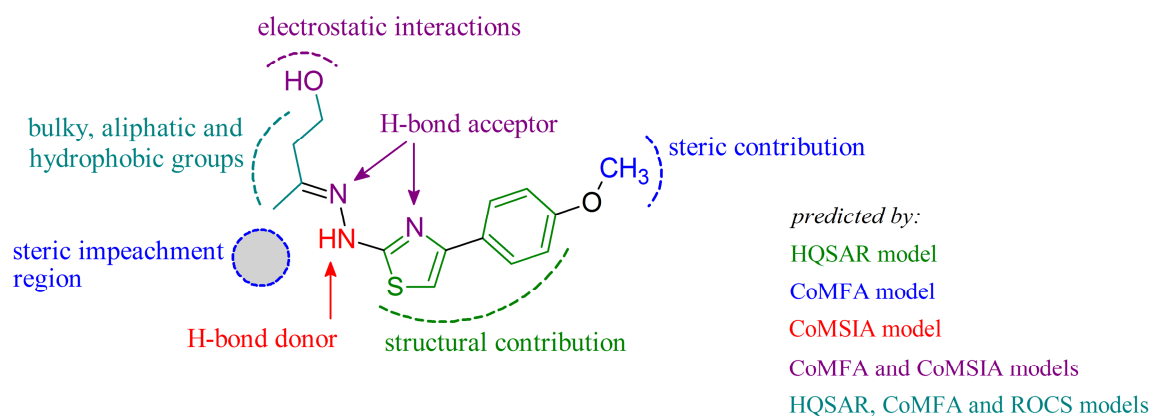


Figure 9 - Main observed features from HQSAR, CoMFA, CoMSIA and ROCS models.

4. Conclusions

Evaluation of *in vitro* antifungal activity of novel hydrazine thiazoles revealed that several of them showed potent activity against clinically important *Candida* and *Cryptococcus* species, with MIC values ranging from low micromolar to nanomolar. These results demonstrate the significant potential of this class of compounds as antifungal agents. In addition, the active compounds showed low cytotoxicity to human embryonic kidney cells.

All generated QSAR and similarity models were robust and have high predictive power in performed validations. Furthermore, all models were employed to provide physicochemical interpretations, which corroborated experimental SAR studies and, therefore, they can be employed in the design of new antifungal agents. Further synthesis followed by molecular modeling studies will be carried out to increase the antifungal potency of hydrazine-thiazole derivatives. In this sense, new QSAR models can be generated using compounds **10-15** in training set, as well as, planned derivatives in order to increase applicability domain of proposed models. Both generated 2D- and 3D-QSAR models presented satisfactory internal and external validations parameters and further studies could increase the accuracy of models and increase the range of prediction for new compounds.

Conflict of interest

The authors state that they have no conflict of interest.

Acknowledgements

The authors thank the Fundação de Amparo à Pesquisa de Minas Gerais (FAPEMIG), Conselho Nacional de Desenvolvimento Científico e Tecnológico (CNPq) and Coordenação de Aperfeiçoamento de Pessoal de Nível Superior (CAPES) for financial support. The authors thank also Centro de Pesquisas René Rachou (FIOCRUZ) for providing high-resolution mass-spectra and OpenEye Scientific Software for OMEGA and ROCS academic licenses.

References

- [1] D.A. Enoch, H. Yang, S.H. Aliyu, C. Micallef, The changing epidemiology of invasive fungal infections, *Methods Mol. Biol.* 1508 (2017) 17-65. Doi: 10.1007/978-1-4939-6515-1_2
- [2] Ravikant, T. Kaur, S.Gupte, M. Kaur, A review on emerging fungal infections and their significance, *J. Bacteriol. Mycol.* 1 (2015) 1-3. Doi: 10.15406/jbmoa.2015.01.00009
- [3] L.C. Whitney, T. Bicanic, Treatment principles for *Candida* and *Cryptococcus*, *Cold Spring Harb. Perspect. Med.* 10 (2014) a024158. Doi: 10.1101/cshperspect.a024158

- [4] P.G. Pappas, C.A. Kauffman, D.R. Andes, C.J. Clancy, K.A. Marr, L. Ostrosky-Zeichner, A.C. Reboli, M.G. Schuster, J.A. Vazques, T.J. Walsh, T.E. Zaoutis, J.D. Sobel, Clinical practice guideline for the management of candidiasis: 2016 update by the Infectious Diseases Society of America, *Clin. Infect. Dis.* 62 (2016) e1–50. Doi: 10.1093/cid/civ933
- [5] A.L. Colombo, T. Guimarães, T. Sukienik, A.C. Pasqualotto, R. Andreotti, F. Queiroz-Telles, S.A. Nouér, M. Nucci, Prognostic factors and historical trends in the epidemiology of candidemia in critically ill patients: an analysis of five multicenter centers sequentially conducted over a 9-year period, *Intensive Care Med.* 40 (2014) 1489–98. Doi: 10.1007/s00134-014-3400-y
- [6] A.M. Doi, A.C.C. Pignatari, M.B. Edmond, A.R. Marra, L.F.A. Camargo, R.A. Siqueira, V.P. da Mota, A.L. Colombo, Epidemiology and microbiologic characterization of nosocomial Candidemia from a Brazilian National Surveillance Program, *PLoS ONE.* 11 (2016) e0146909. Doi:10.1371/journal.pone.0146909
- [7] R. Kaur, M.S. Dhakad, R. Goyal, R. Kumar, Emergence of non-albicans *Candida* species and antifungal resistance in intensive care unit patients, *Asian Pac. J. Trop. Biomed.* 6 (2016) 455-460. Doi: <http://dx.doi.org/10.1016/j.apjtb.2015.12.019>
- [8] A.V. Ferreira, C.G. Prado, R.R. Carvalho, K.S. Dias, A.L. Dias, *Candida albicans* and non-*C. albicans* species: comparison of biofilme production and metabolic activity in biofilms, and putative virulence properties of isolates from hospital environments and infections, *Mycopathologia.* 175 (2013) 265-272. Doi: 10.1007/s11046-013-9638-z.
- [9] E.K. Maziarz, J.R. Perfect, Cryptococcosis, *Infect. Dis. Clin. North Am.* 30 (2016) 179–206. Doi: 10.1016/j.idc.2015.10.006
- [10] R. Rahasubgham, R.M. Smith, B.J. Park, J.N. Jarvis, N.P. Govender, T.M. Chiller, D.W. Denning, A. Loyse, D.R. Boulware, Global burden of disease of HIV-associated Cryptococcal Meningitis: an updated analysis, *Lancet Infect. Dis.* 17 (2017) 873-881. Doi: 10.1016/S1473-3099(17)30243-8
- [11] M.A. Shikanai-Yasuda, R.P. Mendes, A.L. Colombo, F. Queiroz-Telles, A.S.G. Kono, A.M.M. Paniago, A. Nathan, A.C.F.D. Valle, E. Bagagli, G. Benard, M.S. Ferreira, M.M. Teixeira, M.L. Silva-Vergara, R.M. Pereira, R.S. Cavalcante, R. Hahn, R.R. Durlacher, Z. Khoury, Z.P. Camargo, M.L. Moretti, R. Martinez, Brazilian guidelines for the clinical management of Paracoccidioidomycosis, *Rev. Soc. Bras. Med. Trop.* 50 (2017) 715-740. Doi: 10.1590/0037-8682-0230-2017
- [12] R. Martinez, New trends in Paracoccidiomycosis epidemiology, *J. Fungi* 3 (2017), 1-13. Doi: [10.3390/jof3010001](https://doi.org/10.3390/jof3010001)
- [13] H.C. de Oliveira, P.A. Assato, C.M. Marcos, L. Scorzoni, A.C. de Paula e Silva, J.F. da Silva, J.L. Singulani, A.M. Fusco-Almeida, M.J. Mendes-Giannini, Paracoccidioides-host

interaction: an overview on recente advances in the Paracoccidioidomycoses, *Front. Microbiol.* 6 (2015) 1319. Doi: 10.3389/fmicb.2015.01319

[14] T. Roemer, D.J. Krysan, Antifungal drug development: challenges, unmet clinical needs, and new approaches, *Cold Spring Harb. Perspect. Med.* 4 (2014) a019703. Doi: 10.1101/cshperspect.a019703

[15] D. Sanglard, Emerging threats in antifungal-resistant fungal pathogens, *Front. Med.* 3 (2016) 11. Doi: <https://doi.org/10.3389/fmed.2016.00011>

[16] T.I. de Santana, M.O. Barbosa, P.A.T.M. Gomes, A.D.N. da Cruz, T.G. da Silva, A.C.L. Leite, Synthesis, anticancer activity and mechanism of action of new thiazole derivatives, *Eur. J. Med. Chem.* 144 (2018) 874-886. Doi: <https://doi.org/10.1016/j.ejmech.2017.12.040>

[17] P.A.T.M. Gomes, M.O. Barbosa, E.F. Santiago, M.V.O. Cardoso, N.T.C. Costa, M.Z. Hernandes, D.R.M. Moreira, A.C. Silva, T.A.R. Santos, V.R.A. Pereira, F.A.B. Santos, G.A.N. Pereira, R.S. Ferreira, A.C.L. Leite, New 1,3-thiazole derivatives and their biological and ultrastructural effects on *Trypanosoma cruzi*, *Eur. J. Med. Chem.* 121 (2016) 387-398. Doi: <https://doi.org/10.1016/j.ejmech.2016.05.050>

[18] T.A. Farghaly, M.A. Abdallah, M.A. Khedr, H.K. Mahmoud, Synthesis, antimicrobial activity and molecular docking study of thiazole derivatives, *J. Heterocyclic Chem.* 54 (2017) 2417-2425. Doi: 0.1002/jhet.2838

[19] F. Chimenti, B. Bizzarri, A. Bolasco, D. Secci, P. Chimenti, A. Granese, S. Carradori, M. D'Ascenzio, D. Lilli, D. Rivanera, Synthesis and biological evaluation of novel 2,4-disubstituted-1,3-thaizoles as anti-*Candida* spp. Agents, *Eur. J. Med. Chem.* 46 (2011) 378-382. Doi: 10.1016/j.ejmech.2010.10.027

[20] N.P. de Sá, C.I. Lino, N.C. Fonseca, B.M. Borelli, J.P. Ramos, E.M. Souza-Fagundes, C.A. Rosa, D.A. Santos, R.B. de Oliveira, Thiazole compounds with activity against *Cryptococcus gattii* and *Cryptococcus neoformans in vitro*, *Eur. J. Med. Chem.* 102 (2015) 233-242. Doi: 10.1016/j.ejmech.2015.07.032

[21] P. Jirásek, S. Amslinger, J. Heilmann, Synthesis of natural and non-natural curcuminoids and their neuroprotective activity against glutamate-incudec oxidative stress in HT-22 cells, *J. Nat. Prod.* 77 (2014) 2206-2217. Doi: 10.1021/np500396y

[22] J.R. Falck, A. He, L.M. Reddy, A. Kundu, D.K. Barma, A. Bandyopadhyay, S. Kamila, R. Akella, R. Bejot, C. Mioskowski, Ring expansion/homologation – aldehyde condensation cascade using *tert*-trihalomethylcarbinols, *Org. Lett.* 8 (2006) 4445-4647. Doi: 10.1021/ol061953q

[23] N.P. Buu-Hoi, N.D. Xuong, N.B. Tien, Compounds of potential interest for the chemotherapy of leprosy, *J. Org. Chem.* 21 (1956) 415-418. Doi: 10.1021/jo01110a010

- [24] I.N. Klochkova, A.A. Anis'kov, Intramolecular heterocyclization of α,β -unsaturated ketone thiosemicarbazones, *Russ. J. Org. Chem.* 45 (2009) 146-150. Doi: 0.1134/S1070428009010205
- [25] C. de Monte, S. Carradori, D. Secci, M. D'Ascenzio, P. Guglielmi, A. Mollica, S. Morrone, S. Scarpa, A.M. Aglian, S. Giantulli, I. Silvestri, Synthesis and pharmacological screening of a large library of 1,3,4-thiadiazolines as innovative therapeutic tools for the treatment of prostate cancer and melanoma, *Eur. J. Med. Chem.* 105 (2015) 245-262. Doi: 10.1016/j.ejmech.2015.10.023
- [26] S. Carradori, D. Secci, A. Bolasco, D. Rivanera, E. Mari, A. Zicari, L.V. Lotti, B. Bizzarri, Synthesis and cytotoxicity of novel (thiazol-2-yl)hydrazine derivatives as promising anti-Candida agents, *Eur. J. Med. Chem.* 65 (2013) 102-111. Doi:10.1016/j.ejmech.2013.04.042
- [27] M.K. Gupta, A.K. Sachan, S.N. Pandeya, V.S. Gangwar, Synthesis and antibacterial activity of semicarbazones and thiosemicarbazones, *Asian J. Chem.* 19 (2007) 5-9.
- [28] H. Ogura, T. Itoh, T. Okamoto, S. Omura, Nuclear Magnetic Resonance of semicarbazones and thiosemicarbazones of an aliphatic aldehyde, *Chem. Pharm. Bull.* 17 (1969) 844-846. Doi: 10.1248/cpb.17.844
- [29] J. Liu, R. Cao, W. Yi, C. Ma, Y. Wan, B. Zhou, L. Ma, H. Song, A class of potent tyrosinase inhibitors: alkylidenethiosemicarbazide compounds, *Eur. J. Med. Chem.* 44 (2009) 1773-1778. Doi:10.1016/j.ejmech.2008.04.002
- [30] D. Secci, S. Carradori, B. Bizzarri, A. Bolasco, P. Ballario, Z. Patramani, P. Fragapane, S. Vernarecci, C. Canzonetta, P. Filetici, Synthesis of a novel series of thiazole-based histone acetyltransferase inhibitors, *Bioorg. Med. Chem.* 22 (2014) 1680-1689. Doi: 10.1016/j.bmc.2014.01.022
- [31] E. Maccioni, M.C. Cardia, L. Bonsignore, A. Plumitaloo, M.L. Pellerano, A. De Logu, Synthesis and anti-microbial activity of isothiosemicarbazones and cyclic analogues, *Farmaco.* 57 (2002) 809-817. Doi: 10.1016/S0014-827X(02)01288-0
- [32] Clinical and Laboratory Standards Institute. Reference method for broth dilution antifungal susceptibility testing of yeasts, approved standard-Third Ed. CLSI document M27-A3. Wayne: Clinical and Laboratory Standards Institute. (2008).
- [33] S. Johann, M.G. Pizzolatti, C.L. Donnici, M.A. Resende, Antifungal properties of plants used in Brazilian traditional medicine against clinically relevant fungal pathogens, *Braz. J. Microbiol.* 38 (2007) 632-637. Doi: 10.1590/S1517-83822007000400010
- [34] R.C. Hahn, J.S. Handam, Effects of amphotericin B and three azole derivatives on the lipidic of yeast cells of *Paracoccidioides brasiliensis*, *Antimicrob. Agents Chemother.* 44 (2000) 1997-2000.

- [35] R.C. Cruz, S.M.C. Werneck, C.S. Oliveira, P.C. Santos, B.M. Soares, D.A. Santos, P.S. Cisalpino, Influence of different media, incubation times, and temperatures for determining the MICs of seven antifungal agents against *Paracoccidioides brasiliensis* by microdilution. *J. Clin. Microbiol.* 51 (2013) 436-443. Doi: 10.1128/JCM.02231-12
- [36] T. Mosmann, Rapid colorimetric assay for cellular growth and survival: application to proliferation and cytotoxicity assays, *J. Immunol. Methods.* 65 (1983) 55-63. Doi: 10.1016/0022-1759(83)90303-4
- [37] Dassault Systèmes BIOVIA, Discovery Studio Visualizer, v16 1.0, San Diego: Dassault Systèmes, 2015.
- [38] P.C.D. Hawkins, A.G. Skillman, G.L. Warren, B.A. Ellingson, M.T. Stahl, Conformer generation with OMEGA: algorithm and validation using high quality structures from the Protein Databank and Cambridge Structural Database, *J. Chem. Inf. Model.* 50 (2010) 572–584. Doi: 10.1021/ci100031x
- [39] OMEGA 2.5.1.4: OpenEye Scientific Software, Santa Fe, NM. <http://www.eyesopen.com> (2010).
- [40] C.W. Yap, PaDEL-descriptor: an open source software to calculate molecular descriptors and fingerprints, *J. Comput. Chem.* 32 (2011) 1466–1474. Doi: 10.1002/jcc.21707
- [41] C.A. Nunes, M.P. Freitas, A.C.M. Pinheiro, S.C. Bastos, Chemoface: a novel free user-friendly interface for chemometrics, *J. Braz. Chem. Soc.* 23 (2012) 2003-2010. Doi: 10.1590/S0103-50532012005000073
- [42] Tripos Inc. Sybyl-X suite. www.certara.com/software/molecular-modeling (2013)
- [43] K. Roy, K. Supratik, R.N. Das, Statistical methods in QSAR/QSPR, in: K. Roy, K. Supratik, R.N. Das (Eds.), *A Primer on QSAR/QSPR Modeling – Fundamental Concepts*, Springer International Publishing, New York, 2015, pp. 37–59.
- [44] P. Gramatica, A. Sangion, A historical excursus on the statistical validation parameters for QSAR models: a clarification concerning metrics and terminology, *J. Chem. Inf. Model.* 56 (2016) 1127-1131. Doi: 10.1021/acs.jcim.6b00088
- [45] T.I. Netzeva, A. Worth, T. Aldenberg, R. Benigni, M.T. Cronm, P. Gramatica, J.S. Jaworska, S. Kahn, G. Klopman, C.A. Marchant, G. Myatt, N. Nikolova-Jeliazkova, G.Y. Patlewicz, R. Perkins, D. Roberts, T. Schultz, D.W. Stanton, J.J. van de Sandt, W. Tong, G. Veith, C. Yang, Current status of methods for defining the applicability domain of (quantitative) structure-activity relationships, *Altern. Lab. Anim.* 33 (2005) 155-173.
- [46] M.M. Mysinger, M. Carchia, J.J. Irwin, B.K. Shoichet, Directory of useful decoys, enhanced (DUD-E): better ligands and decoys for better benchmarking *J. Med. Chem.* 55 (2012) 6582-6594. Doi: 10.1021/jm300687e

- [47] P.C.D. Hawkins, A.G. Skillman, A. Nicholls, Comparison of shape-matching and docking as virtual screening tools, *J. Med. Chem.* 50 (2007) 74-82, 2007. Doi: 10.1021/jm0603365
- [48] ROCS 3.2.2.2: OpenEye Scientific Software, Santa Fe, NM. <http://www.eyesopen.com>
- [49] A.C. Tenchiu, I.D. Kostas, D. Kovala-Demertzi, A. Terzis, Synthesis and characterization of new aromatic aldehyde/ketone 4-(β -D-glucopyranosyl)thiosemicarbazones, *Carbohydr. Res.* 344 (2009) 1352-1364. Doi: 10.1016/j.carres.2009.05.010
- [50] B. Rupavani, V. Peesapati, V.G.M. Naidu, S. Ramakrishna, Synthesis of some new physiologically active polyheterocycles derived from benzocyclohepten-5-ones, *Indian J. Chem.* 55B (2016) 88-93.
- [51] F. Chimenti, B. Bizzarri, E. Maccioni, D. Secci, A. Bolasco, R. Fioravanti, P. Chimenti, A. Granese, S. Carradori, D. Rivanera, D. Lilli, A. Zicari, S. Distinto, Synthesis and *in vitro* activity of 2-thiazolylhydrazone derivatives compared with the activity of clotrimazole against clinical isolates of *Candida* spp, *Bioorg. Med. Chem. Lett.* 17 (2007) 4635-4640. Doi: 10.1016/j.bmcl.2007.05.078
- [52] M.C. Gidaro, S. Alcaro, D. Secci, D. Rivanera, A. Mollica, M. Agamennone, L. Giampietro, S. Carradori, Identification of new anti-*Candida* compounds by ligand-based pharmacophore virtual screening, *J. Enzyme Inhib. Med. Chem.* 31 (2016) 1703-1706. Doi: 10.3109/14756366.2016.1156103
- [53] N.P. Sá, C. M. Lima, C.I. Lino, P.J.S. Barbeira, L.M. Baltazar, D.A. Santos, R.B. Oliveira, E. Mylonakis, B.B. Fuchs, S. Johann, Heterocycle thiazole compounds exhibit antifungal activity through increase in the production of reactive oxygen species in the *Cryptococcus neoformans-Cryptococcus gatti* species complex, *Antimicrob. Agents Chemother.* 25 (2017) e02700-16. Doi: 10.1128/AAC.02700-16

- Fifteen hydrazine-thiazole derivatives were synthesized.
- The compounds were evaluated against clinically important *Candida* and *Cryptococcus* species.
- Eight compounds showed promising antifungal activity (MIC = 0.45 to 31.2 μ M).
- Compounds showed remarkable selectivity compared to human embryonic kidney (HEK-293) cells.
- Molecular modeling studies were also carried out.